Gravity inversion of a complex interface in the presence of interfering sources

Fernando J. S. Silva Dias(*), ON, Valeria C. F. Barbosa, LNCC and João B. C. Silva, UFPA

Abstract

We present a new semi-automatic gravity interpretation method for estimating a complex interface separating two media containing heterogeneities produced by the existence of interfering sources. The method combines a robust fitting procedure and the constraint that the interface is very smooth near the interfering sources whose approximate horizontal coordinates are defined by the user. The proposed method differs from the regional-residual techniques by using no spectral content assumption about the interface to be estimated, i.e., the interface can produce a gravity response containing both low- and high-wavenumber features. As a result, it may be applied to map the relief of a complex interface in a geological setting containing either shallow- or deep-seated interfering sources. Tests with synthetic data have shown that the method can be of utility in estimating the basement relief of a sedimentary basin in the presence of salt layers and domes or in the presence of mafic intrusions in the basement and/or in both basement and sediments. The method was applied to real gravity data from two geological setting having different kind of interfering sources and interface to be interpreted: 1) the anorthositie-tonalite interface over the outcrop East Bull gabbro-anorthosite complex, Ontario, Canada; and 2) the sediments-basement interface over Algarve Basin, south Portugal. The results showed good agreement with the corresponding known geological features, even when the estimated interface and the interfering sources present highly overlapping spectral contents.

Introduction

Most of the gravity methods aiming at the estimation of an interface separating two media either consider both media to be homogeneous or an homogeneous lower medium and an heterogeneous upper medium where the density contrast is assumed to decay with depth only. All these methods are unsuitable to interpret geological settings where one or both media present heterogeneities produced by the existence of interfering sources (salt domes, dikes, or sills, for example). Usually, in this case, the interpreter must perform a preliminary regional-residual separation, by assuming that the regional and residual anomalies are produced, respectively, by a single deep-seated interface and by shallow and small-sized interfering sources, both confined to narrow depth intervals. Among the traditional regional-residual separation methods applied to gravity anomalies the spectral, and the polynomial fitting methods are the most used methods to date. These methods presume that the regional and residual anomalies present non-overlapping spectra so that a judicious cutoff wavenumber may be used to separate both anomalies. In the case of interfering sources spreading over a large depth interval, such as salt diapirs and diabase dikes, the spectral content of both regional and residual anomalies will severely overlap so that any classic regional-residual separation would fail. In this paper we present a new gravity inversion method for mapping a complex interface separating two media in the presence of interfering heterogeneities, in one or both media, whose anomaly spectrum present a non negligible overlap with the spectral content of the interface.

Method

The forward problem - Let $\mathbf{g}^{\mathbf{o}}$ be an N-dimensional vector of gravity observations (Figure 1a) produced by an interface separating two 2D layered media. Both media are homogenous with densities ρ_1 and ρ_2, except for the presence of a few isolated homogeneous domains with arbitrary bounds embedded in each layered media (Figure 1b). To estimate the relief of this interface, a finite region in the space enclosing the interface and the interfering bodies is discretized into M vertical, prisms whose tops are coincident with the Earth surface (Figure 1b). The horizontal dimension of all prisms is constant and known. The prisms thicknesses represent the depths to the interface and are the parameters to be estimated (Figure 1b). The observed gravity anomaly produced by such interface in the presence of interfering geological sources is a superposition of overlapping gravity effects and a noise component such that,

$$\mathbf{g}^{\mathbf{o}} = \mathbf{g}^{\mathbf{R}} + \mathbf{g}^{\mathbf{r}} + \boldsymbol{\varepsilon} \qquad (1)$$

where $\boldsymbol{\varepsilon} \in R^N$ is a vector of random experimental errors, $\mathbf{g}^{\mathbf{R}}$ and $\mathbf{g}^{\mathbf{r}}$ are, respectively N-dimensional vectors of regional and residual gravity fields.

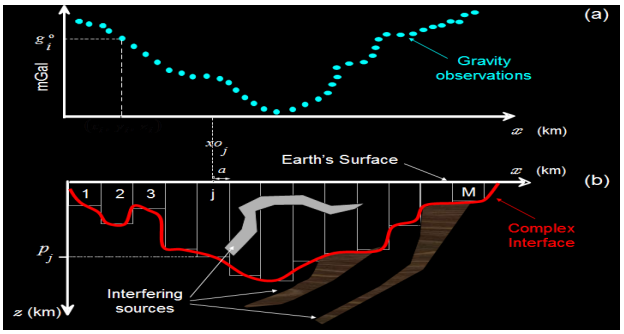

Figure 1 - Interpretation model. (a) Gravity anomaly (blue dots). (b) The geological setting consisting of an interface (red line) and multiple interfering sources (colored polygons). The interpretation model consists of a set of M juxtaposed vertical prisms, whose thickness p_j are the parameters to be estimated.

In this paper, the residual gravity signature is assumed to be produced by the interfering sources. On the other hand, the regional gravity signature is produced by the interface, i.e., the geological feature of our interest. The *i*th observation of the theoretical regional gravity anomaly g_i^R at the *i*th observation point ($x = x_i$, $y = y_i$, and $z = z_i$) is related to the thickness of the *j*th prism (p_j) by the nonlinear relationship

$$g_i^R(x_i, y_i, z_i) = \sum_{j=1}^{M} \Delta\rho_j \gamma \int_{xo_j - a}^{xo_j + a} \int_{-\infty}^{+\infty} \int_{0}^{p_j} \frac{\beta_{ij}}{\left[u_{ij}^2 + v_{ij}^2 + \beta_{ij}^2\right]^{3/2}} dx'\, dy'\, dz', \; i = 1, \ldots, N \quad (2)$$

where $\Delta\rho_j \equiv \Delta\rho \equiv \rho_1 - \rho_2$ is the presumably known density contrast of the *j*th prism, $u_{ij} = x_i - x'_j$, $v_{ij} = y_i - y'_j$, $\beta_{ij} = z_i - z'_j$, γ is Newton's gravitational constant, xo_j is the coordinate of the *j*th prism center, a is the constant half-width of the prisms along the x–direction.

The inverse problem - The nonlinear gravity inverse problem of estimating an M–dimensional vector $\mathbf{p}$, i.e., estimating the depths to the interface at discrete points in the presence of interfering geological sources, is solved by minimizing the functionals

$$\left\| \mathbf{W}_{\mathbf{p}}^{1/2} \mathbf{R}\mathbf{p} \right\|^2, \quad (3)$$

$$\left\| \mathbf{w}_{\mathbf{o}} \mathbf{p} - \mathbf{p}^{\mathbf{o}} \right\|^2, \quad (4)$$

and

$$\left\| \mathbf{W}_{\varepsilon}^{1/2} \mathbf{r} \right\|^2, \quad (5)$$

subject to the positivity constraint on the parameter vector

$$\mathbf{p} \geq \mathbf{0} \quad (6)$$

where $\mathbf{r} = \mathbf{g}^{\mathbf{o}} - \mathbf{g}^{\mathbf{R}}(\mathbf{p})$ is the N-dimensional vector of residual, ||.|| is the Euclidean norm, $\mathbf{R}$ is an $M-1 \times M$ matrix representing the first-order discrete differential operator whose rows contain only two nonnull elements, 1 and -1, which are associated with each pair of adjacent parameters, $\mathbf{p}^{\mathbf{o}}$ is a prior reference vector, $\mathbf{W_o}$ is an $M \times M$ diagonal matrix whose i th diagonal elements may assume only values zero if the corresponding parameter will not be constrained to be close to p_i^o, and one otherwise, $\mathbf{W}_{\varepsilon}$ and $\mathbf{W}_{\mathbf{p}}$ are, respectively, $N \times N$ and $M-1 \times M-1$, diagonal, positive-definite weighting matrices defined in next section.

By assuming $\mathbf{p^o}$ as a null vector, $\mathbf{w_o}$ as a null matrix, $\mathbf{W}_{\varepsilon} = \mathbf{I}_N$ and $\mathbf{W}_{\mathbf{p}} = \mathbf{I}_{M-1}$, where $\mathbf{I}_{\nu}$ is an identity, ν th - order matrix, the estimated interface obtained by minimizing functional (3) subject to the constraint

$$\frac{\| \mathbf{r} \|^2}{N} = \delta^2, \quad (7)$$

is the first–order Tikhonov regularization, where δ^2 is the expected mean-square of the noise realizations in the gravity data. By minimizing $\|\mathbf{Rp}\|^2$ we will favor solutions that are relatively flat and implicitly introduce prior information that the interface is overall smooth (Barbosa et al, 1997). In this paper, the estimation of an interface using the first–order Tikhonov regularization will be referred to as *global smoothness* (GS) inversion. The GS inversion is therefore particularly suited to interpret a smooth interface separating two homogeneous media. However, it is not appropriate to map an interface in the presence of multiple interfering sources. In this case, the GS solution in the neighborhood of the interfering sources becomes severely biased toward a spurious interface, which may be shallower or deeper than the true interface. According to equation (5), matrix $\mathbf{W}_{\varepsilon}$ controls the proximity between the observed and fitted data. If $\mathbf{W}_{\varepsilon} = \mathbf{I}_N$, the sum of squared difference between the observed and fitted data must be close to zero in the least-squares sense. In this paper, however, to produce a more robust data fitting than least-squares' fit, in the class of *M* estimators (Huber, 1981), $\mathbf{W}_{\varepsilon}$ is not defined as the identity matrix. The *i*th diagonal element of $\mathbf{W}_{\varepsilon} \equiv \{ W_{\varepsilon_{ii}} \}$ is defined as being inversely proportional to the *i*th residual r_i at the *i*th observation. Since $\mathbf{W}_{\varepsilon}$ is a function of $\mathbf{r}$, a robust data fitting is implemented in practice by iteratively updating the parameter estimates and the values of $w_{\varepsilon_{ii}}$. Small weights are assigned to large residuals and vice-versa. In this method, the objective of introducing functional (3) is twofold: i) it produces a stable solution; ii) it minimizes the influence of the interfering sources (residual sources) on the estimated interface (regional source). To meet the second objective, matrix $\mathbf{W}_{\mathbf{p}}$ is used to enhance the smoothness of the interface in the neighborhood of the interfering source, by weighting the *i*th row of $\mathbf{R}$ by the *i*th diagonal element of $\mathbf{W}_{\mathbf{p}} \equiv \{ w_{p_{ii}} \}$ which is assigned a sufficiently large number. Finally, as will be shown in next section, minimizing functional (4) forces that the estimated interface about the interfering source, be approximated by a first-degree polynomial.

The proposed methodology was implemented in two steps using a semi-automatic method by assuming that the approximate horizontal coordinates positions, xc_{φ}, $\varphi = 1, \cdots, \Phi$, of Φ interfering sources, are either known a priori or estimated via a preliminary inversion of the gravity data. In the first step, we use the GS inversion to obtain the estimate $\hat{\mathbf{p}}^{\mathbf{GS}}$ as the unconstrained minimizer of

$$\phi_1(\mathbf{p}) = \frac{\|\mathbf{r}\|^2}{N} + \lambda^s \|\mathbf{Rp}\|^2, \quad (8)$$

where λ^S is a nonnegative scalar. In the second step, we implement an iterative process using $\hat{\mathbf{p}}^{\mathbf{GS}}$ as the initial approximation and minimize functionals (3), (4) and (5), that is, we minimize functional

$$\phi_2(\mathbf{p}) = \left\| \mathbf{W}_{\varepsilon}^{1/2} \mathbf{r} \right\|^2 + \lambda^{ws} \left\| \mathbf{W}_{\mathbf{p}}^{1/2} \mathbf{R}\mathbf{p} \right\|^2 + \lambda^o \left\| \mathbf{w}_{\mathbf{o}} \mathbf{p} - \mathbf{p}^{\mathbf{o}} \right\|^2 \quad (9)$$

subject to the inequality constraint (6), which was introduced in our inverse problem through the least

squares algorithm with nonnegativity constraints (Haskell and Hanson, 1981). Parameters λ^o and λ^{ws} are nonnegative scalars. The vector $\mathbf{p}^o$ and the matrices $\mathbf{W}_\varepsilon$, $\mathbf{W}_\mathbf{p}$, and $\mathbf{W}_\mathbf{0}$ are given in the next section.

Mathematical and computational details of the method - Assume a set of S_φ, $\varphi = 1, \cdots, \Phi$, interfering sources, each one characterized by a horizontal coordinate xc_φ and a region around this coordinate, referred to as the φth *interfering region*, defined as follows.

At the first step, by minimizing the functional $\phi_1(\mathbf{p})$ [equation (8)] with respect to $\mathbf{p}$ we obtain the GS solution $\hat{\mathbf{p}}^{\mathbf{GS}}$. Using $\hat{\mathbf{p}}^{\mathbf{GS}}$ solution, we identify the estimated interface concavity at $(xo_j, \hat{p}_j^{GS})$, $j = 2,3,..., M-1$ as upward or downward, respectively, depending on which inequality,

$$\hat{p}_j^{GS} > \frac{\hat{p}_{j-1}^{GS} + \hat{p}_{j+1}^{GS}}{2}, \qquad (10)$$

or

$$\hat{p}_j^{GS} < \frac{\hat{p}_{j-1}^{GS} + \hat{p}_{j+1}^{GS}}{2} \qquad (11)$$

hold. Then, for each interference $S_\varphi, \varphi = 1, \cdots, \Phi$, we identify the coordinate xo_j from the set $\{xo_k\}, k = 1, \cdots, M$ which is closest to xc_φ and determine the x–coordinates, xo_{φ_I} and xo_{φ_F}, closest to xo_j such that at all points inside the interval $[xo_{\varphi_I}, xo_{\varphi_F}]$ containing xo_j, the estimated interface curvature (downward or upward) is the same as the curvature at xo_j. Indices φ_I and φ_F refer to the leftmost and rightmost x-coordinates of the φth *interfering region* (Figure 2).

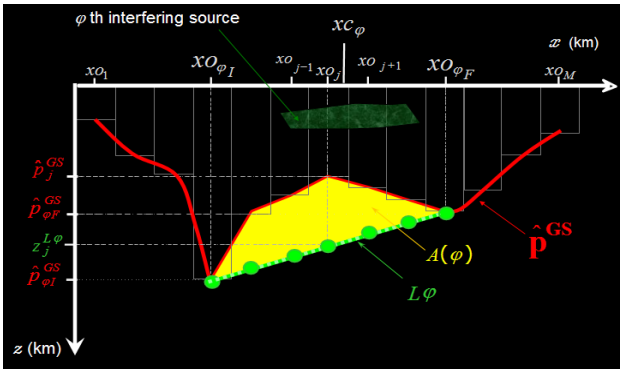

Figure 2 - Schematic representation of the φth interfering region defined by any coordinate xc_φ inside it and by the interval $x \in [xo_{\varphi_I}, xo_{\varphi_F}]$. The elements used to automatically define vector $\boldsymbol{p^o}$ and matrix $\mathbf{W}_\mathbf{p}$ are the φth straight line, L_φ, (green line), the area $A(\varphi)$ (yellow area) and the depths $z_j^{L\varphi}$ of the line L_φ at $xo_j \in [x\varphi_1, x\varphi_2]$ (green dots).

At the second step, we minimize functional $\phi_2(\mathbf{p})$ [equation (9)] using $\hat{\mathbf{p}}^{\mathbf{GS}}$ as the initial approximation and defining the vector $\mathbf{p}^\mathbf{o}$ and the matrices $\mathbf{W}_\varepsilon$, $\mathbf{W}_\mathbf{p}$ and $\mathbf{W}_\mathbf{0}$ in the following way. For $j = 1,..., M$, if xo_j lies outside any interfering region, we set $p_j^o = 0$ and $\mathbf{W}_\mathbf{0} \equiv \{w_{o_{jj}}\} = 0$. Likewise, for $i = 1,..., N$, if the coordinate $x = x_i$ of the ith observation lies outside any interfering region, we set $\mathbf{W}_\varepsilon \equiv \{w_{\varepsilon_{ii}}\} = 1$. Finally, for $j = 1,..., M-1$, if the coordinate $\frac{xo_{j+1} + xo_j}{2}$ lies outside any interfering region, we set $\mathbf{W}_\mathbf{p} \equiv \{w_{\mathbf{p}_{jj}}\} = 1$. Otherwise, for $j = 1,..., M$, if the coordinate xo_j lies inside any interfering region, we set $\mathbf{W}_\mathbf{0} \equiv \{w_{o_{jj}}\} = 1$. Matrix $\mathbf{W}_\mathbf{p}$ and vector $\mathbf{p}^\mathbf{o}$ are obtained in the following way. We first define L_φ as the straight line joining the coordinates $(xo_{\varphi_I}, \hat{p}_{\varphi_I}^{GS})$ to $(xo_{\varphi_F}, \hat{p}_{\varphi_F}^{GS})$ (green line, Figure 2). Next, we determine the area $A(\varphi)$ (yellow area, Figure 2) of the φth interfering area bounded by the straight line L_φ and by the segment of the current estimated interface defined by points $(xo_j, \hat{p}_j^{GS})$, $j = \varphi_I, \varphi_{I+1}, ..., \varphi_F$. For $j = 1,..., M-1$, if the coordinate $\frac{xo_{j+1} + xo_j}{2}$ lies inside the φth interfering area, the jth diagonal element of $\mathbf{W}_\mathbf{p}$ is given by

$$\mathbf{W}_\mathbf{p} \equiv \{w_{\mathbf{p}_{jj}}\} = \left(\frac{A(\varphi)}{A_{\max}}\right) \cdot \alpha \qquad (12)$$

where α is a positive number varying from 30 to 300 and $A_{\max} = \max_{1<\varphi\leq\Phi}[A(\varphi)]$. For $j = 1,..., M$, if the coordinate xo_j lies inside the φth interfering region, we set the jth element of $\mathbf{p}^\mathbf{o}$, p_j^o, to the z–coordinate $z_j^{L\varphi}$ of the intersection of L_φ with the vertical line $x = xo_j$. Figure 2 shows (green dots), the elements assigned to $\mathbf{p}^\mathbf{o}$ for the φth interfering region. Finally, we update matrix $\mathbf{W}_\varepsilon$ in the following way. If the ith observation point at $x = x_i$ lies inside the φth interfering region, the ith diagonal element of matrix $\mathbf{W}_\varepsilon$, at the kth iteration of the second step of our method, is

$$\mathbf{W}_\varepsilon \equiv \{w_{\varepsilon_{ii}}^k\} = \left(10\,(e^{-0.5 r_i^{(k-1)}/s_i^{(k-1)}}) + 0.01\right)/10\,, \qquad (13)$$

where $r_i^{(k-1)}$ is the ith absolute value of the residual at the $(k-1)$st iteration, defined as the difference between the ith observation and the gravity effect at the same point produced by the interface estimated at the $(k-1)$st iteration, and $s_i^{(k-1)}$ is the median of the absolute value of all residuals r_i, $i = 1,..., N$, computed at the $(k-1)$st iteration. Note that the elements of matrix $\boldsymbol{W_p}$ associated with a large interfering region are assigned a large value [see equation (12)] while those elements which are not associated with any interfering region are set to unit. This abrupt transition between the elements of matrix $\boldsymbol{W_p}$, which is associated with the neighborhood of the border

of an interference region, leads to the presence of spurious spikes on the estimated interface relief. To prevent the occurrence of such undesirable features, we introduced a smooth transition between the elements of matrix $\boldsymbol{W_p}$ associated with the neighborhood of the borders of interfering regions. Different degrees of smoothness may be introduced. We assumed the smallest degree of smoothness capable of eliminating any spurious spike on the estimated interface relief. Finally, we note that whereas matrix $\boldsymbol{W\varepsilon}$ is iteratively updated according to equation (13), matrices $\boldsymbol{W_p}$ and $\boldsymbol{W_o}$ are kept fixed for all the subsequent iterations.

Tests with synthetic data

Salt domes as interfering sources - Figure 3a shows a set of noise-corrupted Bouguer anomaly observations (dots) produced by a 2D sedimentary basin (Figure 3b) consisting of homogeneous sediments (gray area) containing a salt layer and intruded by salt diapers (white area). The sediments and the salt units are assumed to have uniform density contrasts of -0.2 g/cm^3 and -0.4 g/cm^3, respectively, relative to a homogeneous basement (black area). The actual basement relief shows, in the interval $x \in [25\,\text{km}, 95\,\text{km}]$ a smooth behavior producing a gravity response with a low-wavenumber spectral content. However, the structural high around $x = 18$ km yields a gravity response with a high-wavenumber spectral content which might be interpreted as a residual anomaly due to a shallow interfering source. On the other hand, the gravity response of the interfering sources (salt layer and domes) has a spectral content ranging from low to high wavenumbers. We use 62 juxtaposed, vertical prisms with widths of 2 km, assume the correct density contrast $\Delta\rho$ of -0.2 g/cm^3 between the sediments and the basement and set, $\lambda^s(\delta) = 50$, $\lambda^{ws}(\delta) = 0.1$, $\lambda^o(\delta) = 14$, $\alpha = 50$, $N_\varphi = 2$, $xc_1 = 46$, and $xc_2 = 67$. Figure 3b shows the estimated interface (red line) evidencing the good performance of our method in estimating both the flat area and the high-amplitude undulations of the interface. The fitted anomaly is shown in Figure 3a (red line). For comparison, we also estimated the basement relief using the GS inversion [minimizer of functional (8)] applied to the regional anomalies estimated by least-squares and by robust polynomial fitting methods. The former will be referred to as GS_LSP inversion and the latter as GS_RP inversion. Figure 3a shows the estimated gravity effect of the basement topography by fitting the seventh-degree polynomial to the gravity data using the Beltrão et al.'s (1991) robust regional-residual separation method (green line) and the standard least-squares method (yellow line). We assume an interpretative model and a density contrast ($\Delta\rho = -0.2$ g/cm^3) identical to the ones used in the previous test. Figure 3b shows the basement relief estimated via the GS_RP (green line) and the GS_LSP (yellow line) inversions, by setting $\lambda^s(\delta) = 5$ and $\lambda^s(\delta) = 6$, respectively. By comparing the inversion results shown in Figure 3b, we note that the proposed method has a superior performance in defining the basement relief as compared with the GS_LSP and GS_RP inversions. This happens because our method *i*) does not assume a priori premises about signal spectral content of the interface to be estimated, i.e., the interface can be characterized by both low- and high-wavenumbers; and *ii*) relies on the interpreter's ability and a priori information to differentiate between the high-wavenumber features which belong to the interface from those originated a posteriori, which characterize the interference.

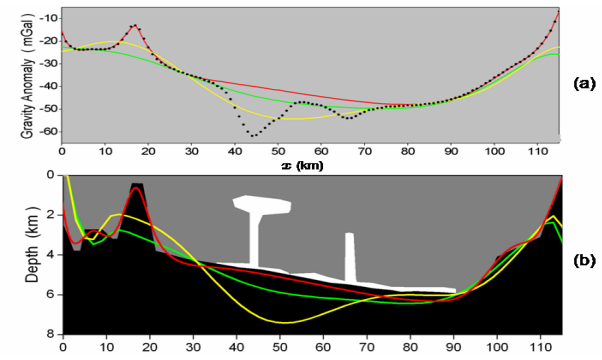

Figure 3 – Simulated salt domes as interfering sources. (a) Noise-corrupted Bouguer (dots) and fitted (red line) anomalies. The regional fields separated from the gravity field by least-squares (yellow line) and robust (green line) methods using a polynomial of degree 7. (b) The true basement relief is represented as the contact separating the gray (sediments) and black (basement) areas. The salt domes represent the interfering sources (white areas). The basement relief estimated by the proposed method (red line), the GS_RP (green line), and the GS_LSP (yellow line) inversions.

Igneous intrusions as interfering sources - Figure 4a displays the noise-corrupted gravity anomaly (dots) produced by a 2D sedimentary basin (Figure 4b) consisting of basement (black area) and sediments (gray area), both intruded by interfering sources simulating intrusive structures such as dikes and sills (white area). The uniform density contrasts of the sediments and the intrusive sources relative to the basement are -0.2 g/cm^3 and 0.13 g/cm^3, respectively. The residual interfering sources (intrusive structures) are located both above and below the regional source (basement relief). We inverted this anomaly using an interpretation model consisting of 86 vertical prisms with widths of 3 km. Figure 4b shows, in red line, our inversion result by setting $\lambda^s(\delta) = 30$, $\lambda^{ws}(\delta) = 4$, $\lambda^o(\delta) = 0$, α=20, N_φ=2, $xc_1 = 110$, and $xc_2 = 186$, and assuming the correct density contrast of -0.2 g/cm^3 between sediments and basement. The fitted anomaly is shown in Figure 4a (red line). We also compare our basement relief estimate with those obtained by the GS inversion applied to the regional fields separated from the gravity field by the least-squares (yellow line, Figure 4a) and robust (green line, Figure 4a) fitting methods using a seventh degree polynomial. Figure 4b shows the basement relief estimated by the GS_RP (green line) and GS_LSP (yellow line) inversions by setting $\lambda^s(\delta)$=15 and $\lambda^s(\delta)$=5, respectively. A comparison between our result (red line, in Figure 4b) and those using the GS inversion applied to the regional anomalies separated by regional-residual polynomial fittings (green and yellow lines in Figure 4b) shows the better performance of our method in recovering the basement topography marked by both the smooth and the non-smooth sections of the interface.

The results using GS_RP (green line) and GS_LSP (yellow line) inversions, on the other hand, do not resolve the basement structures, including the gravity effect with high-wavenumber spectral content, associated with, the steep topography at $x = 150$ km.

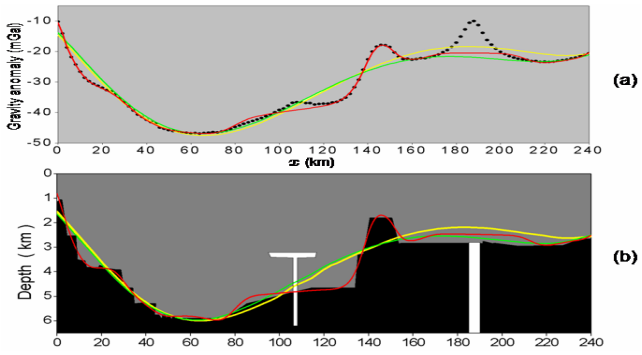

Figure 4 – Simulated igneous intrusions as interfering sources. (a) Noise-corrupted Bouguer (dots) and fitted (red line) anomalies. The regional fields separated from the gravity field by least-squares (yellow line) and robust (green line) methods using a polynomial of degree 7. (b) The true basement relief is represented as the contact separating the gray (sediments) and black (basement) areas. The igneous intrusions represent the interfering sources (white areas). The basement relief estimated by the proposed method (red line), the GS_RP (green line) and the GS_LSP (yellow line) inversions.

Tests with real data

East Bull intrusion - Figure 5a displays the gravity anomaly (dots) over the layered East Bull Lake Gabbroic-Anorthositic Intrusion, Ontario, Canada (Paterson and Reeves, 1985). It is produced by a gabbroic rock embedded in larger anorthositic source. Both units are embedded in a tonalitic host rock. We applied our methodology to this anomaly with the purpose of estimating the interface separating the anorthositic from the tonalitic units. We established an interpretation model consisting of 60 prisms with width of 0.1 km. Based on outcrop information about the known extent of the gabbroic rocks, we assume the presence of just a single interfering source $(N_\varphi = 1)$ at $xc_1 = 3.35$ km and set $\lambda^s(\delta) = 3$, $\lambda^o(\delta) = 0$, and $\alpha = 3$. The assigned density contrast between the anorthositic and tonalitic rocks was 0.2 g/cm^3. Figure 5b shows the estimated anorthositic-tonalitic interface (contact separating the gray and black areas). The fitted anomaly is shown in Figure 5a (solid black line). Figure 5a shows the regional anomalies estimated by the least-squares (solid gray line) and robust (dashed gray line) polynomial fitting methods using a polynomial of seventh degree. Figure 5b shows the anorthositic-tonalitic estimated interface using the GS_LSP (solid line) and GS_RP (dashed line) inversions, and setting $\lambda^s(\delta) = 15$. Both interfaces estimated via GS_LSP and GS_RP inversions show just a slightly deeper low close to $x = 3.2$ km as compared with our inversion method at the same point, which estimated a low having a flat bottom whose maximum depth attains 0.35 km. So, our method as well as the GS_LSP and GS_RP inversions interpreted the feature about $x = 3.2$ km as the gravity effect of the grabbroic unit which outcrops in the interval $x \in [2.3, 3.8]$ km. On the other hand, at $x = 2.2$ km our inversion estimated a noticeable oscillation of the anorthositic-tonalitic interface whereas the estimated interface by both GS_LSP and GS_RP inversions display at the same point a manifest smoothness. We stress that our method introduces a high degree of smoothness in the estimated interface close to the interfering source (outcropping gabbroic rocks), without, however, imposing the same characteristic on the rest of the interface. In this way, our method preserved the interface oscillation at $x = 2.2$ km and eliminated the influence of the gabbroic source around $x = 3.2$ km. On the other hand, the polynomial separation methods do not yield a regional component characterized by both high- and low-wavenumber spectral contents. As a result, the estimated interfaces by both GS_LSP and GS_RP inversions exhibit the same degree of smoothness everywhere, leading to an overall smooth anorthosite-tonalite interface. Figure 5c shows the results of the Paterson and Reeves's(1985) interactive modeling. They set 2.65 g/cm^3 for the tonalitic country rocks (black area), 2.85 g/cm^3 for the anorthositic rocks (dark gray area), and 2.93 g/cm^3 to the gabbroic rocks (light gray area). The main difference between the Paterson and Reeves's (1985) interpretation and our inversion lies in the interval $x \in [2.5\text{ km}, 4\text{ km}]$ where our method estimates a slightly wider, deeper and flatter anorthositic-tonalitic interface (white line, Figure 5c). On the other hand, we estimated the anorthosite lateral borders very close to the ones presented by Paterson and Reeves's (1985).

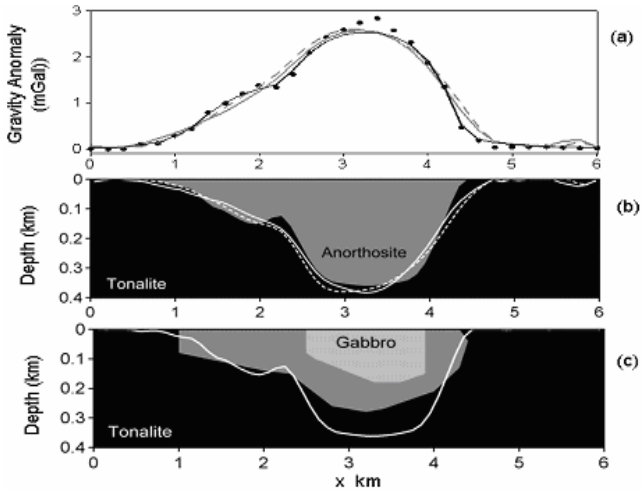

Figure 5 – The anorthosite-tonalite interface over the East Bull complex. (a) Observed Bouguer anomaly (dots) and fitted (solid black line) anomalies. The regional fields separated from the gravity field by least-squares and robust methods using a polynomial of degree 7 are shown in solid and dashed gray lines, respectively. (b) Estimated anorthositic-tonalitic interface using the proposed method (contact between the gray and black areas), the GS_RP inversion (dashed line), and the GS_LSP inversion (solid line). (c) Anorthositic-tonalitic interface estimated by the proposed method (white line) and Paterson and Reeves's (1985) interactive modeling showing the contacts between the tonalite (black area), anorthosite (dark gray area), and gabbro (light gray area).

Algarve Basin - Figure 6a displays the Bouguer anomaly profile (dots) over the offshore Algarve Basin, Gulf of Cadiz, Portugal, corrected for the southwestern crustal thinning effect. At the southeastern portion of the profile in Figure 6a, the gravity high coincides with the structural feature named Guadalquivir Bank (GB), a well-known Paleozoic basement high in Gulf of Cadiz (Maldonado, et al., 1999). Most of Algarve sedimentary basin is covered by multichannel seismic profiles; however, a difficulty in using these data to understand the tectonic structure and the Palaeozoic basement framework is the presence of Triassic and Jurassic salt formations because they attenuate the seismic signal of the basement. We applied the proposed method to the Algarve anomaly to estimate the Palaeozoic Algarve basement relief in the presence of known salt formations which are considered interfering sources. We assumed an interpretation model consisting of 81 vertical prisms with widths of 1 km, density contrast of -0.29 g/cm^3 between the sediments and the basement and set $\lambda^s(\delta)=25,\ \lambda^{ws}(\delta)=6,\ \lambda^o(\delta)=0,$ and $\alpha=7$. Based on the estimated interface at the first iteration, which uses the GS inversion (not shown) we assumed the presence of three interfering source $(N_\varphi=3)$ at $xc_1=8$ km, $xc_2=25$ km, and $xc_3=45$ km. The inversion result is shown in Figure 6b where the Algarve basement relief is delineated by the contact between the black and white areas. The fitted anomaly is shown in Figure 6a (solid line). The results show a structural basement high in the southeastern portion which coincides with the well-known Guadalquivir Bank (GB). Around the coordinates $x=25$km and $x=45$km our method has clearly identified the presence of interfering sources (salt formations) producing large negative residual values. Despite the prior information about the possible existence of interfering source at the coordinate $x=8$km, our method did not yield large negative residuals at this point, indicating that the presented method does not introduce artifacts. Because the test using synthetic data, shown in Figure 3, has been inspired in the Algarve's geology, we are confident that the regional anomaly shown in Figure 6 may have been reasonably well extracted from the observed Bouguer anomaly and that the estimated basement topography is reasonably close to the real topography.

Conclusions

We presented a gravity inversion method for mapping a complex interface separating two media in the presence of multiple interfering sources in one or both media. Weaker restrictions are made about the spectral content of the regional or residual anomalies caused by the interface and the interferences, respectively, as compared with the current regional-residual separation methods. The gravity response of each interference, however, must be either entirely concave or entirely convex. The proposed inversion method combines a robust fitting procedure, consisting of the iteratively re-weighted least-squares method, with the incorporation of the highest degree of smoothness on the estimated interface in the neighborhood of the interfering sources whose approximate horizontal coordinates are defined by the interpreter. In the case of interferences produced by highly magnetic rocks, the discrimination of the features belonging to the interface from those considered to be interference, could be assisted by comparison of gravity with magnetic data if the latter exist. The knowledge about the interfering source's horizontal location may be guessed from the analysis of the interface estimated by a global smoothness method. The proposed method may applied to a variety of geological problems, including the estimation of a sedimentary basin basement topography, delineation of the crust-mantle interface, and delimiting the contact between layered igneous rocks.

References

Barbosa, V. C. F., J. B. C Silva, and W. E. Medeiros, 1997, Gravity inversion of basement relief using approximate equality constraints on depths: Geophysics, **62**, 1745-1757.

Beltrão, J. F., J. B. C. Silva, and J. C. Costa, 1991, Robust polynomial fitting for regional gravity estimation: Geophysics, **56**, 80-89.

Haskell, K. H. and, R. J. Hanson, 1981. An algorithm for linear least squares problems with equality and nonnegativity constraints, Mathematical Programming, **21**, 98-118.

Huber,P.J.,1981, Robust Statistics. Wiley, New York, 308.

Paterson, N. R., and C. V. Reeves, 1985, Applications of gravity and magnetic surveys: The state-of-the-art in 1985: Geophysics, **50**, 2558–2594.

Maldonado, A., L. Somoza, and L. Pallarés, 1999, The Betic orogen and the Iberian–African boundary in the Gulf of Cadiz: geological evolution (central North Atlantic). Marine Geology, **155**, 9-43.

Acknowledgments

This study was supported by the Primeiros Projetos grant by FAPERJ (E-26/170.733/2004). We thank Ms Hugo Matias for the enthusiastic discussions about the geology of the Algarve Basin. J.B.C.S. and V.C.F.B. were supported by fellowships from CNPq. Additional support for J.B.C.S. and V.C.F.B. was provided by CNPq under contracts: 505265/2004-4 and 504419/2004-8. V.C.F.B. was also supported by CNPq (472229/03-6).

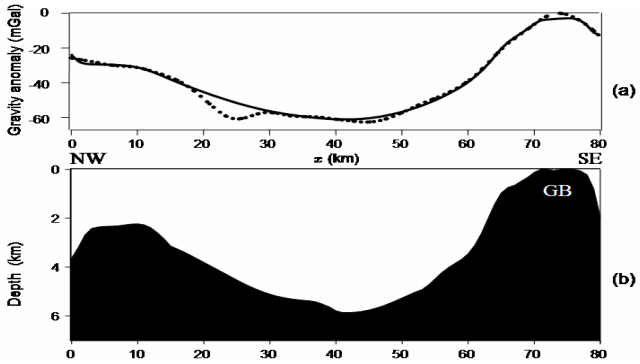

Figure 6 – The sediments-basement interface in the presence of salt formation over Algarve Basin. (a) Observed Bouguer anomaly (dots) and fitted (solid line) anomalies. (b) The estimated Algarve basement relief is shown as the contact separating the white (sediments) and black (basement) areas. GB stands for Guadalquivir Bank.